Chapter 5
Mass Exchange in Dead Water Zones: A Numerical Approach

Luiz E. D. de Oliveira and Johannes G. Janzen

Abstract Dead water zones (DWZs) in natural open channels, formed by consecutive groynes, are regions separated from the main channel, characterized by recirculating flows. These regions present lower velocities compared to the main channel, increasing the deposition of sediment and the temporary storage of polluted materials. Exchange processes between DWZs and the main channel influence the transport of pollutants in channels. This study adopts the k-omega shear stress transport (SST) turbulence model to examine the mass exchange between the main channel and the DWZ created by an infinite series of groynes. The computational results were compared to data collected in literature. A good agreement was achieved in the mass exchange coefficient, with a relative error of approximately 2%.

Introduction

In fluvial engineering, channels are generally shaped by complicated boundaries that can be composed by dead water zones (DWZ), which can be formed by consecutive groynes (Xiang et al. 2019). Groynes are transversal dykes placed in sequence along riverbanks to keep the flow away from the banks. The effects of this structure in rivers are an increase in mean velocity and water depth in the main channel, improved navigability, increased efficiency of sediment transport, protection against flooding and the mitigation of bank erosion (McCoy et al. 2008). Its placement also provides lateral heterogeneity that can favour the presence of aquatic organisms, improving

L. E. D. de Oliveira (✉) · J. G. Janzen
Graduate Programme in Environmental Technologies. Coffee Lab, Engineering, Architecture and Urban Planning and Geography College, Federal University of Mato Grosso Do Sul, Campo Grande, Brazil
e-mail: luedoliveira@gmail.com

J. G. Janzen
e-mail: johannesjanzen@gmail.com

W. Leal Filho and J. B. S. de Andrade Guerra (eds.), *Water, Energy and Food Nexus in the Context of Strategies for Climate Change Mitigation*, Climate Change Management,
https://doi.org/10.1007/978-3-030-57235-8_5

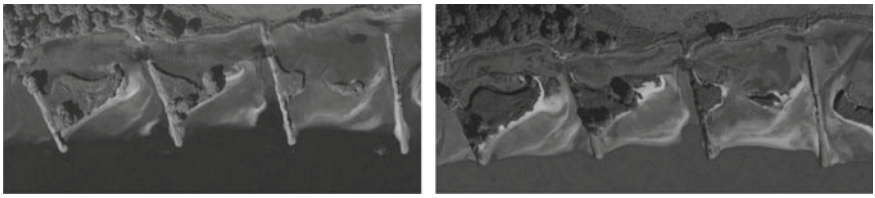

Fig. 5.1 Groyne fields bathymetry change (left) December 2008 (Google Earth Pro 2018) (right) December 2009 (Google Earth Pro 2018)

the biodiversity of river ecosystems (McCoy et al. 2008, 2015; Buczyński et al. 2017; Mignot et al. 2017; Buczyńska et al. 2018; Xiang et al. 2019).

Since the magnitude of mean flow velocities inside the DWZ is approximately 25% of the flow velocities in the main channel, not only the deposition of sediment is enhanced, but also that of nutrients and contaminants which are readily attached to fine particles (Sukhodolov 2014). For instance, the attachment of contaminants to particles was observed in the Middle Elbe River, in Germany, leading to a low standard classification from an ecological view (Schwartz and Kozerski 2003). The authors found, in the groyne fields, the deposition of fresh organic mud with high nutrient and pollution content (e.g. nitrogen). The deposition of pollution content attached to sediments creates a problem for river management (Uijttewaal 2005), especially in flood seasons, when the groyne field becomes submersed, being a source of contaminants to the main channel.

The exchange processes at the groyne field-channel interface can substantially modify the transport and dispersion of contaminants (Constantinescu et al. 2009). It is important to understand, then, how the pollutant cloud interacts with the groyne fields, the storage time and how the pollutants tends to settle. Quantitative knowledge of the exchange processes allows a better estimation of global pollutant spread, which can be used in forecasting models for water quality and river pollution (Weitbrecht et al. 2008). Furthermore, it can indicate a life cycle of groyne fields, as with time it becomes more and more shallow (Fig. 5.1 Left and Right).

Therefore, in order to estimate the transport of pollutants in a channel, it is important to be able to understand and predict the exchange processes between the main channel and the DWZ formed between groynes (Weitbrecht and Jirka 2001). These exchange processes were studied in detail in a series of laboratory experiments carried out by Weitbrecht (2004). Hinterberger et al. (2007) used large eddy simulation (LES) to model Weitbrecht's experimental results. Although it is a very precise model, the LES is also more time consuming when compared to simpler models. Therefore, this study aims to investigate the mass exchange between the main channel and the groyne field using a simpler two-equations turbulence model, k-omega SST. The computational results are compared to Weibrecht's results and a good agreement was obtained.

Methods

The geometry was chosen to match the groynes from the second series of experiments described in Weitbrecht (2004). The flow depth (h) was kept constant at 0.046 m and the experimental channel width (B) at 1.80 m. The emergent groynes were 0.50 m long (W) and spaced 1.25 m apart (L), producing an aspect ratio of $W/L = 0.40$. The groyne heads were in a semi-circle format with a diameter of 0.05 m. The Reynolds number was 7360, and thereby turbulent.

The flow past the most downstream-located groyne in the series had a periodic behaviour (Hinterberger et al. 2007). Consequently, the flow from only one complete groyne field and two halves (located upstream and downstream from the complete one) were computed and a translational periodic boundary condition was imposed (Fig. 5.2). The mean streamwise velocity in the computational domain was approximately $U = 11$ cm/s, which corresponds to a mass flux of 6.56 kg/m^2 of water in the periodic zones.

As the effects of the obstacles in the main channel extend up to one obstacle length in the transversal direction (y-axis) (Brevis et al. 2014) the domain was two-thirds of the experimental flume width (B), reducing the computational effort. A free-slip symmetry boundary condition was imposed on the surface (Fig. 5.2). This boundary condition was also used on the free surface plane, as it is an acceptable simplification for flows with Froude numbers smaller than 0.5 (our Froude number was 0.24) (Alfrink and van Rijn 1983). All walls, bed, lower side wall and groyne walls were considered hydraulically smooth.

The domain was calculated in a three-dimensional grid (Fig. 5.3a). The spatial discretization had a higher refinement in regions close to walls and at high velocity gradient regions. The meshing of the groyne's heads considered its curvature and the proximity to the wall. This region used an O-grid with an increasing element size (Fig. 5.3b). The mesh had 20 divisions in the z-axis, increasing gradually from the

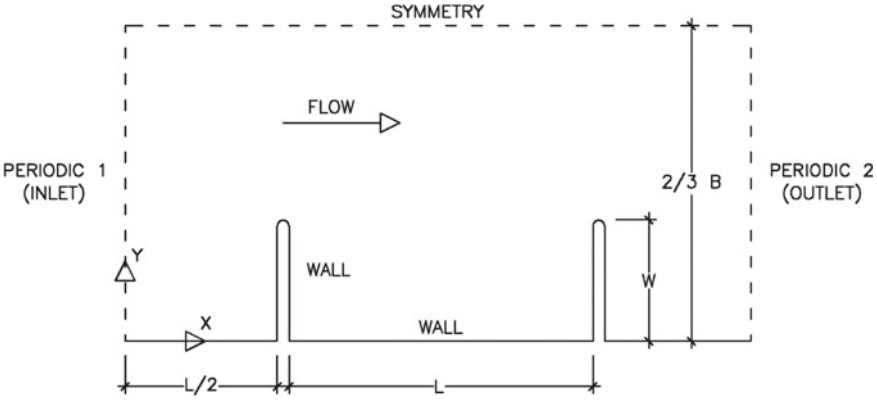

Fig. 5.2 Upper view of the computational domain, from the free surface, and its boundary conditions

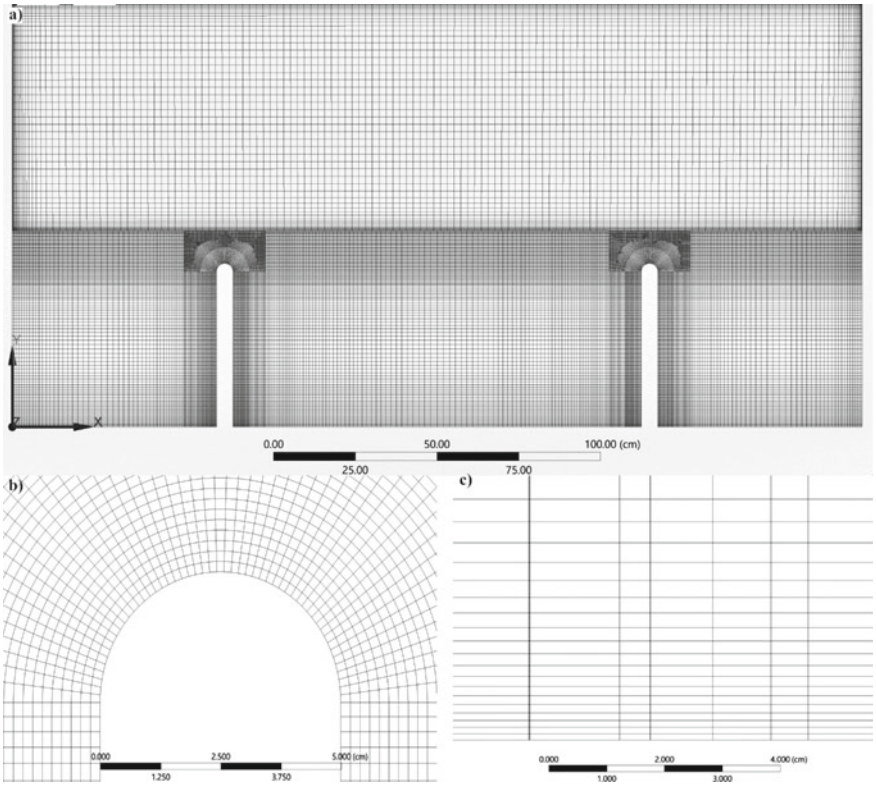

Fig. 5.3 Computational mesh: **a** mesh in the free-surface plane; **b** curvilinear grid around groyne tip; **c** mesh in a vertical plane near the middle of the groyne field

bottom of the channel to its free surface (Fig. 5.3c). In the y-axis, the groyne field had 70 divisions that gradually increased in size as they get closer to the middle of the field. The strip that contains the groyne's heads had finer elements due to the momentum transfer in the shear layer. The total grid presented approximately one million elements.

The commercial software called Ansys® FLUENT (version 14) was used to solve the grid, using the finite volume method to discretize the governing mass and momentum equations. The turbulent model chosen is based on the Reynolds-averaged Navier–Stokes equations (RANS) approach, that consists of time-averaged equations for fluid flow. The turbulent calculations were solved using the k-omega SST model proposed by Menter et al. (2005), due to its capability of solving fluid flow in low Reynolds numbers. The pressure–velocity coupling method was SIMPLE and the gradient spatial discretization was Least Squares Cell Based. The momentum was discretized in a third order MUSCL scheme. The turbulent kinect energy (k) and specific dissipation rate (omega) were discretized in a second order upwind scheme.

In addition to the velocity field, tracer concentration fields were also calculated by solving the following transport equation

$$\frac{\partial}{\partial t}(\rho Y_i) + \nabla.\left(\rho \overrightarrow{v} Y_i\right) = \nabla\left(\rho D_{i,m} + \frac{\mu_t}{Sc_t}\right)\nabla Y_i \tag{5.1}$$

$$Sc_t = \frac{\mu_t}{\rho D_t} \tag{5.2}$$

where ρ is the fluid mass density, Y_i is the local mass fraction of each species, $D_{i,m}$ is the mass diffusion coefficient for species in the mixture, ν is the velocity vector, $D_{i,m}$ the mass diffusion coefficient for species in the mixture, Sc_t is the turbulent Schmidt number (5.2) ($Sc_t = 0.7$), μ_t turbulent viscosity and D_t the turbulent diffusivity. In other terms, the transport equation means that the rate of change and the net rate of flow (convection) equals the rate of change due to diffusion.

Equation (5.1) does not consider any chemical reactions or addition of phases during the solution and was discretized in a second order upwind scheme. The tracer was conservative, pursuing the same properties as water.

The time step in the simulation was 0.024 h/U. The simulation was run for nearly 180 h/U until the fully developed state was achieved. Once the flow reached the fully developed state, the tracer mass fraction was set to 1 within the groyne field and 0 in the other parts of the channel. Then, statistics of the mean flow and tracer transport were calculated using the instantaneous flow fields and mean tracer concentration inside the groyne field over the next 548 h/U.

Results and Discussion

Two gyres could be observed in the groyne field: a large primary gyre (right vortex in the central groyne field) and a small secondary gyre in the upstream groyne (Fig. 5.4). The formation of this system occurred from the momentum transferred by the main channel through a mixing layer. As the main flow went downstream, the shear in between zones excited an anticlockwise gyre (primary gyre) that further excited a smaller clockwise circulation (secondary gyre) that had no contact with the main channel. The secondary gyre was smaller in size (approximately 21% of the groyne field area) and velocity magnitudes, when compared to the mean circulation (Fig. 5.4).

Figure 5.5 shows the mean streamwise velocity distributions for $x/L = 0.25$, 0.50 and 0.75 (x has origin in the right face of the first groyne and points to the right). Overall, the model had a good accordance in the main channel and in the central part of the groyne field. The computational model was able to capture the circulation pattern inside the groyne field. However, near the groyne heads (interface between the main channel and the groyne fields) the concordance was not so good. This is due to the high dissipation of momentum that occurred in the mixing layer. Despite the fine resolution of the grid, the model could not describe the flow inside this region.

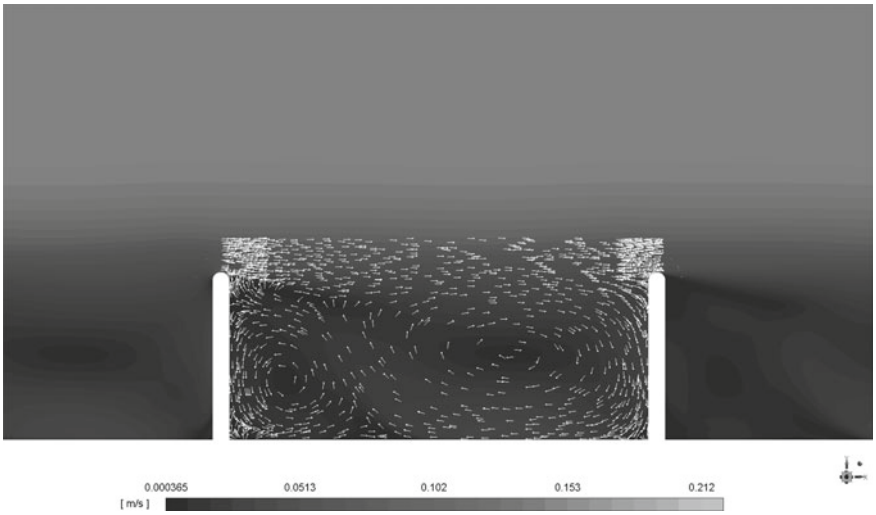

Fig. 5.4 Mean velocity contour

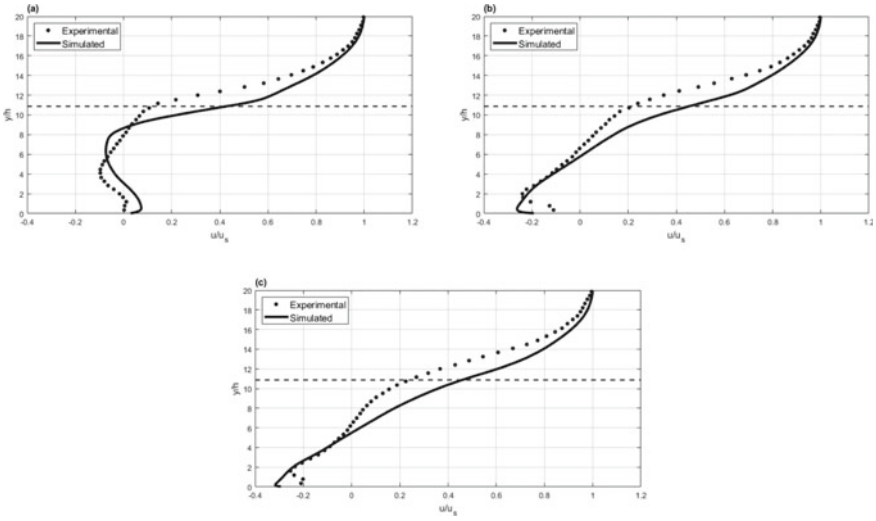

Fig. 5.5 Mean streamwise velocity distributions. **a** $x/L = 0.25$, **b** $x/L = 0.50$ and **c** $x/L = 0.75$. The dashed line represents the groyne head position ($y/h = 10.87$)

For the same reason, the secondary gyre did not have contact with the mixing layer, since this vortex was formed by the dissipation of momentum from the primary gyre. The mean error was approximately 102, 21 and 47% for Fig. 5.5a–c, respectively. However, the flow was in the same order of magnitude as the experimental, which indicates that Fig. 5.4 represents qualitatively, at least, the flow within the region.

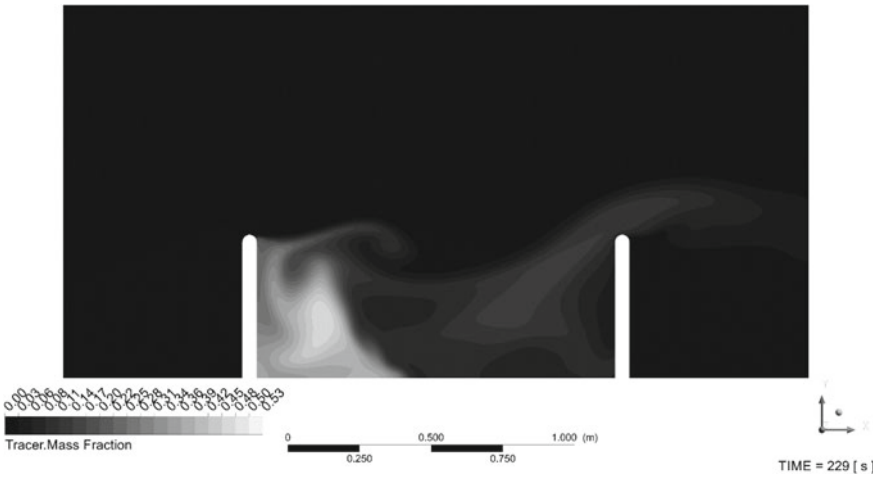

Fig. 5.6 Tracer mass fraction in the free-surface plane in time 229 s

The ejection of tracer from a groyne field to the mixing layer (region between the DWZ and the main channel) occurs in the upstream portion of the field (up to 40%), while the following 60% is a region where mass can re-enter the system (Weitbrecht, 2004). The tracer concentration stayed higher in the secondary gyre, while the primary gyre oscillated due to the injection of tracer from the mixing layer and its natural ejection (Fig. 5.6). This movement was captured by the model and can be seen completely in https://youtu.be/9b-4JZJdeA0.

The tracer concentration inside the field was fitted in a first order decay model (5.3) following the same procedure from the experimental study (Fig. 5.7).

$$C = C_0 \exp(-t/MRT) \tag{5.3}$$

where MRT is the mean retention time. Based on the MRT, the mass coefficient k (5.4) was calculated in order to estimate the intensity of mass exchange (Weitbrecht and Jirka, 2001).

$$k = \frac{W}{MRTU} \tag{5.4}$$

The fitted curve presented an $MRT = 117.7$ s that related to an exchange coefficient of $k = 0.026$. The relative error between the mean value of Weitbrecht's experiments and our model was 1.99% for the exchange coefficient and 1.69% for MRT (Table 5.1).

Although we could observe a good agreement between our computational model and the experimental results, it can be observed that the system presented two slopes, with a breakpoint near $C/C_0 = 0.2$ (Fig. 5.7). The first slope was influenced by the

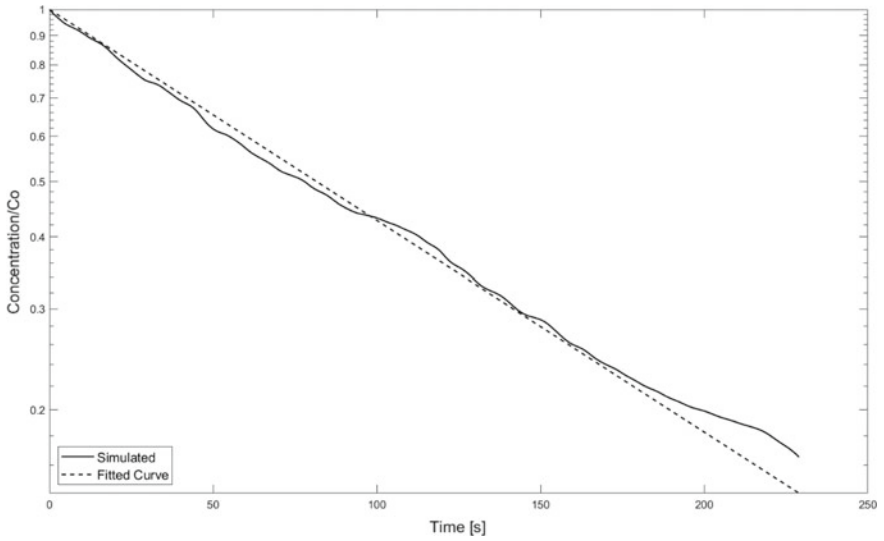

Fig. 5.7 Volumetric averaged mass concentration inside groyne field

Table 5.1 Comparison of mean residence time inside groyne field and exchange coefficient in between experimental and numerical studies

Experiment/Model	MRT [s]	k
Experiment 1	97	0.029
Experiment 2	114	0.028
Experiment 3	125	0.022
Mean value of experiments	118	0.027
3D LES (Hinterberger et al. 2007)	137	0.023
2D LES (Hinterberger et al. 2007)	75	0.042
3D k-omega SST (global fitted curve)	117.7	0.026
3D k-omega SST (first slope)	113.3	0.0274
3D k-omega SST (second slope)	121.62	0.0256

tracer concentration present in the primary gyre, that oscillates between ejecting mass and re-absorbing via the shear layer. The second one ejects mass slower, as the concentration in the field was mainly disposed in the secondary gyre. Figure 5.8 shows the tracer concentration fitted in two curves, the first curve presented an $MRT = 113.27$ s and a $k = 0.0274$ while the second $MRT = 121.43$ s and $k = 0.0256$. The summary of the model and comparisons with previous studies can be seen in Table 5.1.

Our results are consistent with field observations. Sukhodolov et al. (2004), for example, observed that the mass concentrated in the secondary gyre, since it presented the slowest velocities in the groyne field.

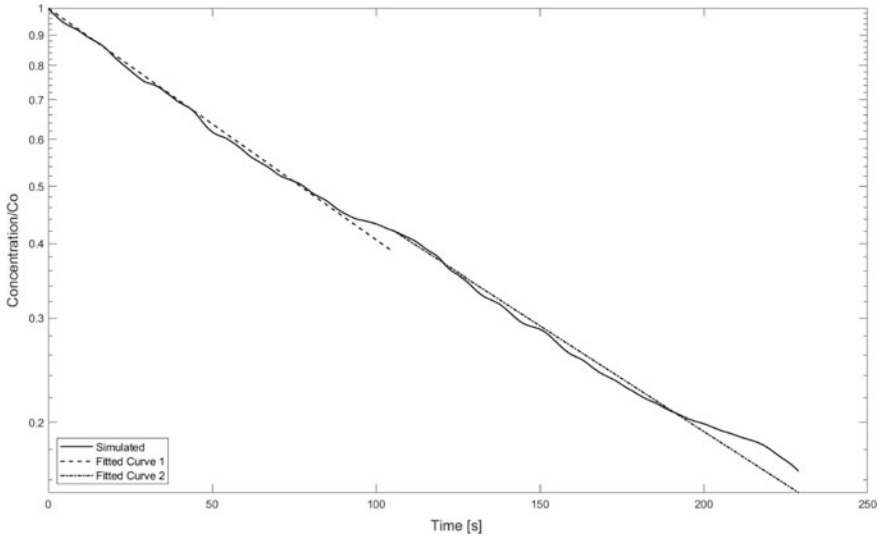

Fig. 5.8 Volumetric averaged mass concentration inside groyne field fitted with two curves

Conclusion

A 3D k-omega SST simulation was presented for a periodic shallow water flow in a groyne field. Our model was able to reproduce a similar structure and magnitude flow compared to experimental data. Furthermore, our model could predict the mass exchange coefficient between the main channel and the DWZ and the mean retention time of the DWZ, being in good concordance with experimental results. In agreement with experimental and field observations, the decay of mass inside the field is described in two phases, first when the primary gyre dominates the ejection and second when the mass is concentrated in the second gyre prolonging the MRT. Hence, a simpler model than LES can predict the main parameters related to the mass exchange process in groyne structures.

Acknowledgements The authors are grateful to members of Coffee Laboratory for providing the necessary hardware. Specifically, D. F. Silva, M. L. M. Xavier, P. H. S de Lima, T. C. R. Ventura and T. N. Yamasaki for research assistance and hardware set up.

Funding
This study was financed in part by the Coordenação de Aperfeiçoamento de Pessoal de Nível Superior—Brazil (CAPES) -Finance Code 001.

References

Alfrink BJ, van Rijn LC (1983) Two-equation turbulence model for flow in trenches. J Hydraul Eng 109(7):941–958. https://doi.org/10.1061/(ASCE)0733-9429(1983)109:7(941)

Brevis W, García-Villalba M, Niño Y (2014) Experimental and large eddy simulation study of the flow developed by a sequence of lateral obstacles. Environ Fluid Mech 14(4):873–893. https://doi.org/10.1007/s10652-013-9328-x

Buczyńska E et al (2018) Human impact on large rivers: the influence of groynes of the River Oder on larval assemblages of caddisflies (Trichoptera). Hydrobiologia 819(1):177–195. https://doi.org/10.1007/s10750-018-3636-6

Buczyński P et al (2017) Groynes: a factor modifying the occurrence of dragonfly larvae (Odonata) on a large lowland river. Mar Freshw Res 68(9):1653–1663. https://doi.org/10.1071/MF16217

Constantinescu G, Sukhodolov A, McCoy A (2009) Mass exchange in a shallow channel flow with a series of groynes: Les study and comparison with laboratory and field experiments. Environ Fluid Mech 9(6):587–615. https://doi.org/10.1007/s10652-009-9155-2

Google Earth Pro (2018) Groyne fields near Hamburg 53°23′54.32″N, 10°11′51.08″E, elevation 1.90 km. Terrain layer, viewed 29 August 2019. https://www.google.com/earth/index.html

Hinterberger C, Fröhlich J, Rodi W (2007) Three-dimensional and depth-averaged large-eddy simulations of some shallow water flows. J Hydraul Eng 133(8):857–872. https://doi.org/10.1061/(ASCE)0733-9429(2007)133:8(857)

McCoy A, Constantinescu G, Weber LJ (2008) Numerical investigation of flow hydrodynamics in a channel with a series of groynes. J Hydraul Eng 134(2):157–172. https://doi.org/10.1061/(ASCE)0733-9429(2008)134:2(157)

Menter FR et al (2005) Transition modelling for general purpose CFD codes. Eng Turbul Model Exp 6(August):31–48. https://doi.org/10.1016/B978-008044544-1/50003-0

Mignot E et al (2017) Measurement of mass exchange processes and coefficients in a simplified open-channel lateral cavity connected to a main stream. Environ Fluid Mech Springer Netherlands 17(3):429–448. https://doi.org/10.1007/s10652-016-9495-7

Schwartz R, Kozerski H-P (2003) Entry and deposits of suspended particulate matter in groyne fields of the middle elbe and its ecological relevance. Acta Hydrochim Hydrobiol 31(45):391–399. https://doi.org/10.1002/aheh.200300496

Sukhodolov AN et al (2004) Case study: turbulent flow and sediment distributions in a groyne field. J Hydraul Eng 130(1):1–19. https://doi.org/10.1061/(asce)0733-9429(2004)130:1(1)

Sukhodolov AN (2014) Hydrodynamics of groyne fields in a straight river reach: insight from field experiments. J Hydraul Res 52(1):105–120. https://doi.org/10.1080/00221686.2014.880859

Szlauer-Łukaszewska A (2015) Substrate type as a factor affecting the ostracod assemblages in groyne fields of the Oder River (Poland). North-Western J Zool 11(2):274–287

Uijttewaal WS (2005) Effects of groyne layout on the flow in groyne fields: laboratory experiments. J Hydraul Eng 131(9):782–791. https://doi.org/10.1061/(ASCE)0733-9429(2005)131:9(782)

Weitbrecht V (2004) Influence of dead-water zones on the dispersive mass transport in rivers. Universitätsverlag Karlsruhe. https://doi.org/10.5445/KSP/1242004

Weitbrecht V, Jirka GH (2001) Flow patterns in dead zones of rivers and their effect on exchange processes. In: International symposium on environmental hydraulics, pp 1–6

Weitbrecht V, Socolofsky SA, Jirka GH (2008) Experiments on mass exchange between groin fields and main stream in rivers. J Hydraul Eng 134(2):173–183. https://doi.org/10.1061/(ASCE)0733-9429(2008)134:2(173)

Xiang K et al (2019) 'Large eddy simulation of turbulent flow structure in a rectangular embayment zone with different population densities of vegetation. Environ Sci Pollut Res 26(14):14583–14597. https://doi.org/10.1007/s11356-019-04709-x